Open Access

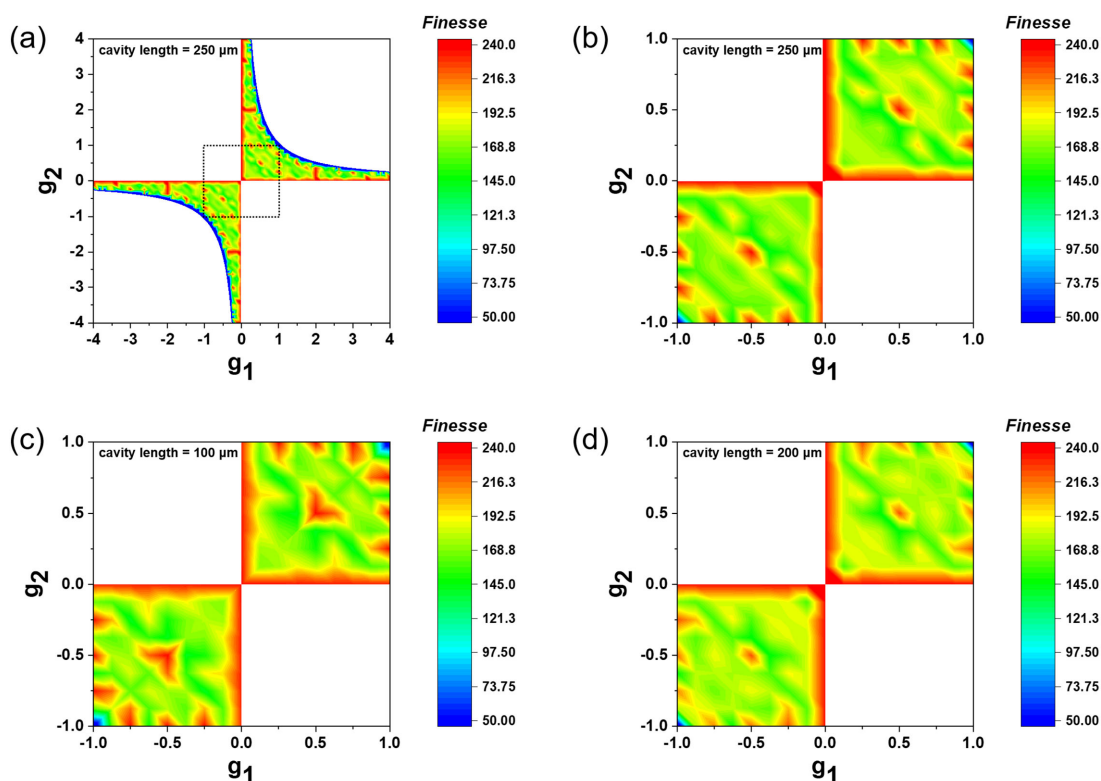# Finesse of Stable Extrinsic Fiber Fabry-Pérot Cavities With Spherical Surfaces

Jiwon Choi
Gyeongho Son
Yeonghoon Jin
Kyoungsik Yu

Finesse of Stable Extrinsic Fiber Fabry-Pérot Cavities With Spherical Surfaces

Jiwon Choi [iD] **, Gyeongho Son, Yeonghoon Jin, and Kyoungsik Yu** [iD]

School of Electrical Engineering, Korea Advanced Institute of Science and Technology,
Yuseong-gu 34141, South Korea

Abstract: In this work, we present a model for spectral transmittance of extrinsic fiber
Fabry-Pérot cavities using paraxial Gaussian approximation and ray transfer matrices. The
finesse is obtained through a Lorentzian fitting of the spectral transmittance derived from
the proposed model. The relationship between the finesse and the radius of curvature on
both sides of the cavity was analyzed to obtain high finesse. The predictions of the model
are found to be in good agreement with the experimental results for the fabricated cavities.

Index Terms: Optical fiber, Fabry-Pérot cavities, resonators, microfabrication.

1. Introduction

Optical Fabry-Pérot cavities (FPCs) have played important roles in optical communication [1],
[2], optical sensors [3]–[5], and quantum electrodynamics [6], [7]. Fiber-based FPCs (FFPCs), in
particular, offer a number of practical advantages, such as affordability, small size, high sensitivity,
immunity to electromagnetic interference, and low insertion loss due to their inherent direct coupling
to the input and output waveguides [3], [8]. The FFPCs can be classified as intrinsic and extrinsic
types depending on whether the light inside the FPC is guided. Extrinsic FFPCs, in which the
light is not strictly guided by the waveguide within the cavity (e.g., free-space propagation between
two cavity mirrors), have been widely used because of their ease of fabrication and their ability
to sense various parameters, such as pressure [9], [10], strain [11], and temperature [12], [13].
A well-known fundamental figure-of-merit for such an extrinsic FFPC is its finesse. Due to the
advantages of having high finesse, there has historically been a great deal of effort to increase this
value. Theoretically, finesse is defined by the effective average number of round-trips of the light
before it leaves the cavity, and this is ultimately limited by the cavity mirror reflectivity for extrinsic
FFPCs. In practice, however, the finesse values are usually affected by a number of non-idealities,
such as the misalignment of the mirrors and inappropriate mirror curvatures. The light diffraction
and beam divergence inside an extrinsic FFPC with finite mirror sizes are also important factors.
While the guided mode radius for the output fiber is fixed, the effective beam size varies inside
the FFPC, which inevitably results in non-ideal output coupling to the output fiber. On this account,
in-depth theoretical modeling for the behavior of the beam propagation inside the extrinsic FFPC

as well as its finesse values considering such diffraction effects has been intensively investigated [14]–[18].

Kilic *et al.* [14] addressed the reflection spectrum of extrinsic FFPCs comprising a single-mode fiber (SMF) and a planar mirror by employing Gaussian beam approximation. They analyzed the origin of the asymmetric Lorentzian profiles in the reflection spectra from the FFPC. In addition, the finesse values were obtained by calculating the round-trip optical losses in consideration of the beam diffraction and the mirror misalignment. Similar studies were also performed by Wilkinson and Pratt [15]. Although these studies are valuable to understand the behavior of extrinsic FFPCs, they are limited to planar-parallel FFPCs.

To address considerable performance degradation in such planar-parallel FPCs, cavity configurations with curved mirrors have been considered [16]–[18]. Various approaches to modeling the behavior of optical beams in such FFPCs have been employed. Sabry *et al.* [16] dealt with an FFPC comprised of a flat dielectric-coated SMF and a concave mirror. They calculated the diffraction losses through round-trip coupling efficiency based on Gaussian approximation. Kleckner *et al.* [17] treated the finesse of FPCs comprised of two concave mirrors through eigenvalues associated with Laguerre-Gaussian modes using the diffraction theory of electromagnetic waves, which was first used by Fox and Li [19]. Benediketer *et al.* [18] employed Hermite-Gaussian mode analysis to determine the finesse of FFPCs comprising a concave machined SMF facet and a plane mirror following the approach of Kleckner *et al.* In all the above studies, the finesse was analyzed according to the cavity length for a specific radius-of-curvature (ROC) of the cavity mirror.

In this paper, a theoretical model is developed that can be used to obtain diffraction-considered spectral transmittance of extrinsic FFPCs, regardless of their mirror curvatures, using the ray transfer matrix approach based on a simple paraxial Gaussian approximation. Using the new model, it is shown that extrinsic FFPCs with finite core dimensions suffer from finesse degradation when compared to conventional planar-parallel cavities with infinite mirror sizes. The effect of the ROC of the cavity mirrors on the finesse values is demonstrated in detail. Finally, the performances of several types of newly fabricated experimental FFPCs were analyzed, and then compared to the theoretical results.

2. Theoretical Model

2.1. Derivation of Spectral Transmittance

Prior to implementing the Gaussian-beam-based model, a conventional description of FPCs with an infinite beam size (plane wave approximation) is discussed first for comparison. A typical FPC consists of two parallel mirrors with infinitely large apertures, and is also referred as an etalon. It is presumed that there are no other optical losses except for the loss due to the reflectivity of the cavity mirrors. As a result, the well-known Airy distribution appears as its spectral response. The conventional formula for the finesse of the standard FPC is given by Eq. (1), which is solely dependent on the reflectivity of the cavity mirrors and sharply increases as the reflectivity increases. In the equation, r_1 and r_2 are the reflectivity of mirror 1 and mirror 2, respectively.

$$F = \frac{\pi}{2\sin^{-1}\left(\frac{1-\sqrt{r_1 r_2}}{\sqrt[4]{r_1 r_2}}\right)} \tag{1}$$

However, in the extrinsic FFPCs with finite mirror sizes, additional losses might occur due to inherent light diffraction. As illustrated in Fig. 1(a), while the light beam from an input fiber reciprocates within the cavity, its beam size changes due to diffraction.

Considering divergence of this beam due to diffraction, the total transmitted electric field E is given by the sum of the multiple waves from the cavity $E = \sum_{n=1}^{\infty} C_n E_{n0}$, where E_{n0} and C_n denote the electric field (complex amplitude) of the nth light arrived at the output fiber side (mirror 2) and the normalized coupling coefficient to the output fiber's propagation mode, respectively. Here, it is assumed that $n = 1$ stands for the case in which light is directly transmitted from the input fiber to the output fiber without any reflections in the cavity. The parameter of C_n can be obtained through
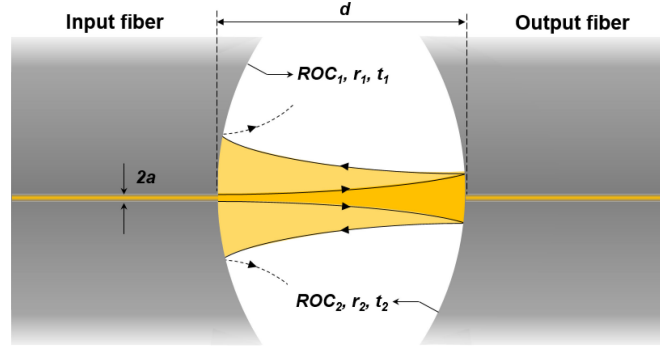
Fig. 1. Illustration of an FFPC with cavity length d comprising two fibers with core radius a, radius of curvature ROC_1 and ROC_2, reflectivity r_1 and r_2, and transmittance t_1 and t_2, respectively. It was assumed that ROC_1 and ROC_2 have positive values in the case of a concave-concave cavity. Note that $r_i + t_i = 1$ holds for $i = 1$ and 2. The initial light direction is left to right and the partial of the beam is reflected between the air and the output fiber interface.

the overlap integral between E_{n0} and E_f, where E_f denotes the propagation mode on the output fiber, and can be obtained in a closed form by assuming that the electric fields are Gaussian (see Appendix A). In this study, we assume that the input and output optical fibers have a finite core size with infinite cladding for simplification. This is a reasonable assumption since the fiber's propagation mode profile is well confined near the core, and does not extend outside the cladding region. Then, the transmitted electric field E could be rewritten as Eq. (2).

$$E = \sum_{n=1}^{\infty} C_n E_{n0} = E_0 \sqrt{t_1 t_2} \sum_{n=1}^{\infty} \frac{2\sqrt{(r_1 r_2)^{n-1}} e^{-jkz_n + j\zeta_n}}{W_n W_f \left(\frac{1}{W_n^2} + \frac{1}{W_f^2} + j\frac{k}{2R_n} \right)} \tag{2}$$

Here, E_0, W_f, W_n, R_n, ζ_n, z_n, and z_{0n} denote the electric field of the light from input fiber, mode radius of the fiber, mode radius, ROC of the wavefront, Gouy phase, propagated axial distance, and Rayleigh range of the beam after n round-trips, respectively. Finally, after some lengthy manipulations, the transmittance of this FFPC is given by Eq. (3).

$$T = \left(\frac{E}{E_0} \right) \left(\frac{E}{E_0} \right)^* = t_1 t_2 \left[\sum_{n=1}^{\infty} \frac{4(r_1 r_2)^{n-1}}{A_{mn}} + \sum_{n=1}^{\infty} \sum_{m=n+1}^{\infty} \frac{8(\sqrt{r_1 r_2})^{n+m-2}}{A_{mn}^2 + B_{mn}^2} (A_{mn} \cos \Theta_{mn} - B_{mn} \sin \Theta_{mn}) \right],$$
$$\tag{3}$$

where $A_{mn} = (W_f/W_n + W_n/W_f) \times (W_f/W_m + W_m/W_f) + k^2 W_f^2 W_n W_m/4R_n R_m$, $B_{mn} = kW_n W_f/2R_n \times (W_f/W_m + W_m/W_f) - kW_m W_f/2R_m \times (W_f/W_n + W_n/W_f)$, and $\Theta_{mn} = (kz_n - \zeta_n) - (kz_m - \zeta_m)$.

The complex Gaussian beam parameters W_n, R_n, z_n, and z_{0n} can be obtained from ray-transfer-matrix analysis (see Appendix B). Assuming that the initial radius of curvature for the Gaussian beam wavefront in the input fiber side is infinite, the initial complex Gaussian beam parameter q_0 in the input fiber is simply given by $q_0 = j(\pi W_f^2/\lambda)$, where W_f represents the effective Gaussian beam radius for the fiber's guided mode. Thus, by using the complex Gaussian beam parameter q_n after multiple round-trips within the cavity (see Appendix C), the other Gaussian beam properties, such as W_n, R_n, ζ_n, and z_n, on the output fiber facet can be obtained. Therefore, the total cavity transmittance shown in Eq. (3) can be obtained from cavity parameters (e.g., cavity length, reflectivity, and ROC as well as beam properties).

3. Discussion

3.1 Verification of the New Model and Lorentzian Fitting

In this study, the finesse was calculated by dividing the free spectral range (FSR) of the Lorentzian fitted curve of the spectral response obtained from the new model by its full-width-at-half-maximum
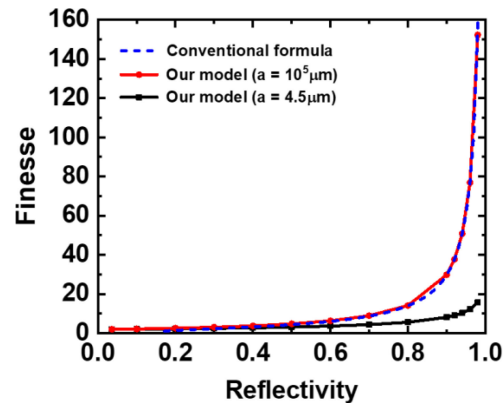
Fig. 2. Cavity finesse as a function of the mirror reflectivity with core radius of 10^5 μm (red curve) and 4.5 μm (black curve) compared with the conventional formula (blue dashed line), which does not consider the diffraction effect.

(FWHM). Unlike the ideal FPC with infinite aperture dimensions, when the beam divergence due to diffraction is considered, the spectral response exhibits asymmetric Lorentzian profiles [14]. Therefore, it is necessary to verify whether the results of the Lorentzian fitting are still valid. The validity of both our model and the Lorentzian fitting are demonstrated by showing that the finesse obtained from the model in an ideal situation without diffraction loss, matches that of the conventional formula. Here, it is assumed that there is no transversal offset and angular misalignment. To eliminate diffraction loss, a collimated beam was created by setting the parameters of the new model. If the core radius of the input fiber is set to have a sufficiently large value, the initial waist radius of the input beam also has a large value. Then, because the beam divergence angle is inversely proportional to the waist radius, the beam rarely diverges and thus becomes a collimated beam. Moreover, if the core radius of the output fiber is set as large as that of the input fiber, the mode radius of the output fiber and of the incident beam become almost the same, thereby minimizing coupling loss due to mode mismatch. Hence, the core radius of the input and output fibers in the model were set sufficiently large, in relation to the cavity length, to make an ideal situation.

Figure 2 shows the finesse values as a function of the mirror reflectivity for planar-parallel FFPCs with two extreme fiber core radii of 4.5 μm and 10^5 μm (almost corresponding to the infinite aperture size). The core radius of 4.5 μm was chosen because it is the typical core radius of the single mode fiber at telecommunication wavelengths. To show how the finesse obtained through our model differs from the ideal situation without any diffraction, we also chose a very large core radius of 10^5 μm. We verified that the simulation results for the finesse values hardly changed when the core radius became sufficiently large, such as 10^5 μm. The cavity length is assumed to be 250 μm. When the core radii of the input and output fiber are 10^5 μm, the finesse values obtained from our model are consistent with the conventional formula, validating our approach.

To find the degree of finesse degradation when diffraction is considered, finesse according to the reflectivity of a cavity surface was obtained when the core radius of the input and output fibers was set to 4.5 μm (corresponding to the single-mode fibers at the telecommunication wavelengths, such as SMF-28). As illustrated in Fig. 2, when the core radius is 4.5 μm, it is confirmed that the finesse degrades over the whole range of reflectivity compared to the ideal situation without any absorption. It is noteworthy that higher reflectivity results in worse finesse degradation according to Fig. 2.
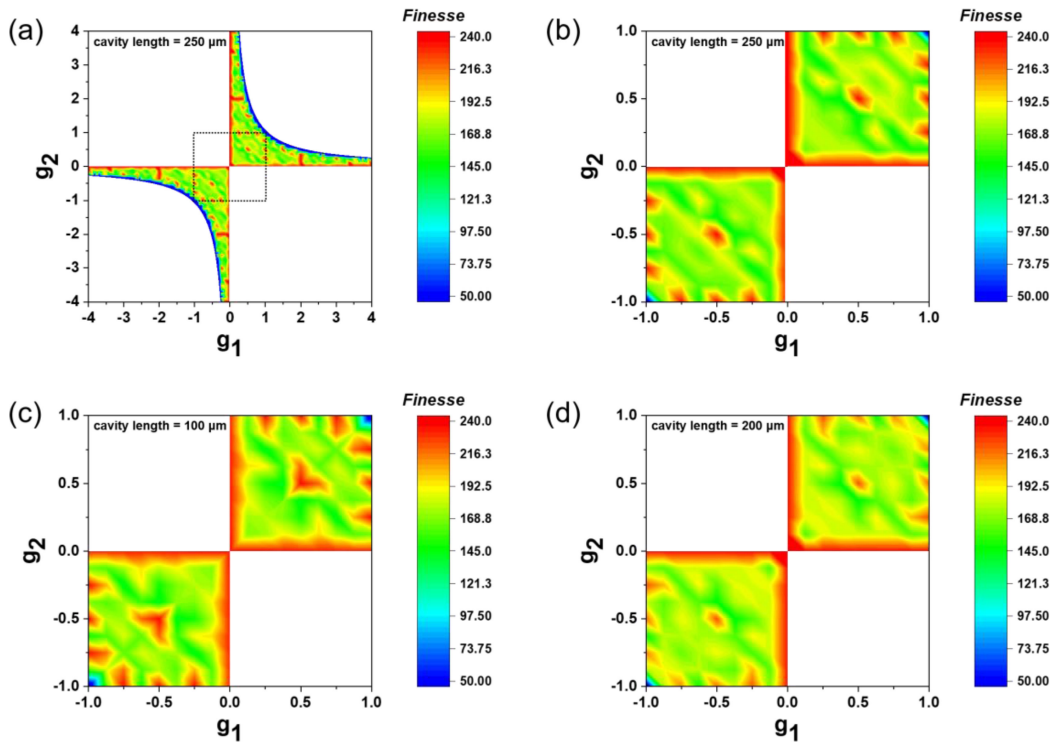
Fig. 3. (a) Finesse of the FFPCs with respect to g_1 and g_2, when the mirror reflectivity is 0.99 and the distance between the two mirrors is 250 μm. The value of g_1 and g_2 represent the stability parameters of each side of the cavity. The finesse for stability parameters g_1 and g_2 (ranging from −4 to 4) are present as contour maps without contour lines. (b) Cavity finesse for g_1 and g_2 with a range of −1 to 1, which is a square part surrounded by the black dotted line in (a). Additional finesse maps of the FFPC with distances of (c) 100 μm and (d) 200 μm.

3.2 Finesse Diagram According to ROC

To address the considerable performance degradation in planar-parallel cavities with finite mirror sizes, there have been many studies on diffraction loss and finesse according to cavity configuration [14]–[20]. Compared to previous studies, we deeply focused on the effects of ROC of cavity surfaces. For extrinsic FFPCs, because the output fiber core dimension (the highly guided region of the beam) is constant, the size of the cavity mirror area was not considered a variable. Instead, the coupling loss due to the mode mismatch between the beam and output fiber was considered for cases where the curvatures of both sides of the cavity had multiple values as independent variables.

Figure 3 shows the finesse of the extrinsic FFPCs with respect to the stability parameter, $g_1 = 1 − d/\text{ROC}_1$ and $g_2 = 1 − d/\text{ROC}_2$, when the mirror reflectivities are $r_1 = 0.99$ and $r_2 = 0.99$, respectively. To investigate the effect of ROCs on the finesse values, the cavity length, d, was first fixed at 250 μm (Figs. 3(a) and (b)). The finesse analysis in Fig. 3(a) was performed on a total of 861 pairs of g_1 and g_2, each having a value in the range −10 to 10 at intervals of 0.125 with stable cavity conditions ($0 \leq g_1 g_2 \leq 1$). Fig. 3(b) shows the enlarged view of the finesse distribution within the range of −1 to 1, signifying the discrete and pseudo-periodic distribution of high finesse configurations. Although the exact finesse values become different with the cavity lengths (Figs. 3(b, c, d)), the overall profiles and the discrete nature of high finesse configurations look similar to each other.

According to Fig. 3, the overall cavity finesse values show symmetric profiles with respect both to the origin and to the line $g_1 = g_2$. Furthermore, high finesse values can be obtained when

$g_1 g_2 = 0$, corresponding to the case of confocal and hemispherical cavity. At the same time, low finesse values are obtained when $|g_1 g_2| = 1$, corresponding to the case of planar-parallel cavity, which is consistent with the previous result [20].

In addition to such high symmetry configurations, a number of configurations have been found to exhibit high finesse values even though they are inside the boundary of the stability diagram. Among symmetric concave-concave cavities, which is a particularly interesting class of extrinsic FFPCs, the configuration with a $|g|$ value of 0.5 showed high finesse. Moreover, for plano-concave cavities, the configurations with $|g|$ values of 0.25, 0.5, and 0.75 on the concave surface showed high finesse. There were also several other configurations with high finesse in the case of the convex-concave cavities. As an example, a high finesse was obtained when the g value of the convex surface was 2, that is, the radius of the convex curvature matches the cavity length.

A common feature of all configurations with the high finesse mentioned above is that the beam radius at the cavity mirror surface remains relatively constant regardless of the number of round-trips, or periodically vary with a specific number of round-trips (constant or oscillating beam size evolution with respect to the number of round-trips within the cavity). Whereas, the low finesse configurations correspond to the case when the beam radius at the cavity mirror surface keeps monotonically increasing with the number of round-trips. These features are directly related to the reason why a particular configuration has higher or lower finesse values in Fig. 3. Recall that the transmitted electric field E could be expressed as the total sum of the product of C_n and E_{n0} at each round-trip, as in Eq. (2). Because $|1/W_n^2 + 1/W_f^2| >> |k/(2R_n)|$ in Eq. (2), W_n at the cavity reflector surface is the main factor determining the magnitude of C_n. Therefore, if W_n remains nearly constant regardless of n, the magnitude of C_n also becomes nearly constant, which results in higher finesse values according to the Fourier transform relationship. Based on the fact that the imaginary part of the inverse of the complex beam parameter is solely dependent on the beam radius, the cavity configurations with nearly constant or periodically-varying beam size can be obtained when $\text{Im}(1/q_n) = \text{Im}(1/q_{n+k})$ from ray-transfer-matrix analysis and complex beam parameters, where q represents the complex beam parameter, and n, k are the positive integer numbers representing the number of round-trips. These configurations are consistent with the configurations with high finesse values shown in Fig. 3.

Compared to the conventional cavity stability diagram without the detailed finesse information, Fig. 3 directly visualize the finesse values according to the wide variety of cavity configuration determined by the ROC and the cavity length as well as the cavity stability. Therefore, the cavity configurations can be more specifically selected. In addition, it was possible to identify several previously unknown configurations that can achieve high finesse from the results obtained in Fig. 3.

4. Experimental Results

4.1 Fabrication

To experimentally verify the validity of our model, four different types of SMF-28-based FFPCs with a combination of flat/curved and uncoated/coated facets were fabricated by chemical wet etching [21] and a subsequent metal deposition process [22]. The wet etching method using hydrofluoric (HF) acid was used to fabricate concave fiber facets [21]. After etching for ~5 min in 49% HF aqueous solution, etched fiber tips were soaked in a beaker containing deionized water for 1 min to prevent unintended additional etching by the residual HF aqueous solution on the fiber surfaces. To enhance the reflectivity of the cavity mirror facets, noble metals (such as Ag and Au) were adopted [22]. Even though its optical loss is much higher than that of dielectric mirrors, the metal deposition (electron beam evaporation) is a cost-effective way to significantly improve the facet reflectivity. Figure 4 shows scanning electron microscope (SEM) images of the metal-coated surfaces (~60 nm of Ag). By combining the etching and deposition processes, four types of fiber facets were produced: uncoated flat, uncoated curved, Ag-coated flat, and Ag-coated curved.
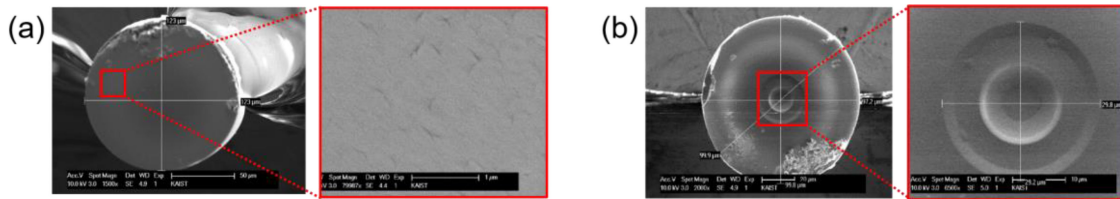
Fig. 4. SEM images of the (a) Flat/Ag-coated and (b) Curved/Ag-coated FFPC surfaces.
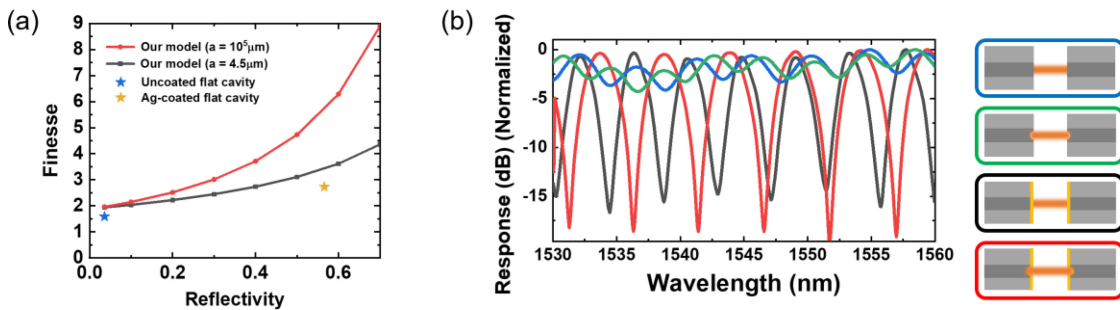

Fig. 5. (a) Experimental results of two fabricated samples. Reflectivity of 0.04 (blue star dot) and 0.58 (yellow star dot) are uncoated and Ag-coated flat cavities, respectively. (b) Measured experimental spectral response of the fabricated extrinsic FFPCs comprising two uncoated flat fibers facets (blue curve), uncoated curved fiber facets (green curve), Ag-coated flat fiber facets (black curve), and Ag-coated curved fiber facets (red curve).

The FFPC's mirror reflectivity was estimated by first measuring the reflectivity at the silica-Ag interface and then considering the difference in the refractive index between silica and air. In order to measure the reflectivity at the silica-Ag interface, the power of light reflected from the Ag-coated fiber facet was measured at a laser wavelength of 1.55 μm using an optical circulator and an optical power meter. The measured reflectivity at the silica (core and cladding)-Ag interface was 43.50%, and the reflectivity at the air-Ag interface was thus estimated to be 56.57%. The reflection from the uncoated flat facet is 3.60%.

4.2 Performance

To create extrinsic FFPCs with submillimeter-scale cavity lengths, two fibers with the same type of facet were configured face-to-face using two V-groove fiber holders, and aligned using multi-axis translational stages. We measured the finesse, quality factor, and visibility of the fabricated FFPCs from the transmission spectra obtained by a combination of a broadband laser source with a wave-length range of 40 nm and an optical spectrum analyzer, as illustrated in Fig. 5. The measurement results are summarized in Table 1. Of these, the finesse values of two FFPCs, each consisting of uncoated flat facets and Ag-coated flat facets, are plotted in Fig. 5(a). The experimentally obtained results similarly follow the monotonically increasing trend of finesse values with respect to the mirror reflectivity. Comparing the experimental values with the values obtained from the conventional formula and our Gaussian-beam-based model, it can be seen that the experimental values are closer to the finesse value obtained from our model considering the diffraction losses, rather than the conventional model. However, the experimental values are still lower than those obtained from our model, which can be attributed to the fact that in addition to the diffraction losses, the finesse values can be further degraded in the actual extrinsic FFPC due to transversal offset and angular misalignment of the cavity mirrors. Furthermore, as can be seen from Table 1, the FFPCs with curved facets showed higher finesse values than a cavity with flat facets. Although the

TABLE 1
Summary of the FFPC Measurement Results

FFPC type	Cavity length* (μm)	Finesse	Quality factor	Visibility (dB)
Uncoated Flat-Flat	261.41	1.59	536.62	4.14
Uncoated Concave-Concave	279.27	1.80	577.45	4.29
Ag-coated Flat-Flat	247.28	2.73	982.16	16.67
Ag-coated Concave-Concave	231.48	4.04	1204.00	19.80

*Cavity length is estimated using the FSR of the spectral response.

reflectivity of the metal coated surfaces used in experiment are different from the simulations and the exact curvature of the cavity facet used in the experiments was not measured, these results are consistent with our model, indicating that having curvature helps improve finesse.

5. Conclusion

In summary, a framework was presented by which to obtain the finesse of extrinsic FFPC. In particular, a spectral transmittance model was developed that considers diffraction based on the paraxial Gaussian approximation. To obtain the beam properties included in the derived spectral transmittance formula, a ray-transfer matrix and complex beam parameter were utilized. It was confirmed that diffraction must be considered in order to achieve a high finesse FFPC by showing that the degradation of finesse due to diffraction becomes more prominent at higher reflectivity. This new framework has the advantage of being able to obtain finesse, even in a cavity with curvature, by a straightforward method. The finesse was shown according to the ROC for a stable FFPC. Configurations able to obtain high finesse, which had not been found in previous studies, were found. Moreover, the reason why high finesse was obtained from those configurations was determined from the viewpoint of coupling efficiency. In the experiment, verification of the new framework was validated by fabricating plane-parallel uncoated and Ag-coated FFPC and comparing it with the results from the new model. In addition, that the concave-concave cavities have better quality factor and visibility than plane-parallel cavities do, was demonstrated experimentally. We expect that the results of this study will contribute to the fabrication of FFPCs with high finesse to meet the increasing demand in various fields such as cavity quantum electrodynamics.

Appendix A
Gaussian Approximation

The input beam can be expressed as a Gaussian beam as shown in Eq. (4).

$$E_n = E_{n0} e^{-\left(\frac{1}{W_n(z)^2} + \frac{jk}{2R_n(z)}\right)r^2 - jkz_n + j\zeta_n} \tag{4}$$

E_{n0} can be expressed as Eq. (5),

$$E_n0 = E_0\sqrt{t_1 t_2}\left(\sqrt{r_1 r_2}\right)^{n-1} \tag{5}$$

Similarly, mode on the output fiber can be expressed as Eq. (6).

$$E_f = E_0 e^{-\frac{r^2}{w_f^2}} \tag{6}$$

C_n can be obtained through Eq. (7).

$$C_n = \frac{\int E_n E_f^* dA}{\sqrt{\int E_n E_n^* dA}\sqrt{\int E_f E_f^* dA}} \tag{7}$$

The normalized coupling coefficient of Eq. (7) can be expressed as Eq. (8) by calculating overlap integral using Eq. (4), (5), and (6).

$$C_n = \frac{2e^{-j(kz_n - \zeta_n)}}{W_n W_f \left(\frac{1}{W_n^2} + \frac{1}{W_f^2} + \frac{jk}{2R_n} \right)} \tag{8}$$

Appendix B
Ray Transfer Matrix

We defined the matrices A, B, C, and D to represent the refraction from the cavity to the output fiber, a single round-trip in the cavity, propagation by cavity length within the cavity, and refraction from the input fiber to the cavity, respectively, and matrices A, B, C, and D can be expressed as Eq. (9),

$$A = \begin{bmatrix} 1 & 0 \\ \frac{1}{ROC_2}\left(1 - \frac{n_{air}}{n_{core}}\right) & \frac{n_{air}}{n_{core}} \end{bmatrix}, B = \begin{bmatrix} 1 & d \\ 0 & 1 \end{bmatrix}\begin{bmatrix} 1 & 0 \\ -\frac{2}{ROC_1} & 1 \end{bmatrix}\begin{bmatrix} 1 & d \\ 0 & 1 \end{bmatrix}\begin{bmatrix} 1 & 0 \\ -\frac{2}{ROC_2} & 1 \end{bmatrix}, C = \begin{bmatrix} 1 & d \\ 0 & 1 \end{bmatrix},$$

$$D = \begin{bmatrix} 1 & 0 \\ \frac{1}{ROC_1}\left(\frac{n_{core}}{n_{air}} - 1\right) & \frac{n_{core}}{n_{air}} \end{bmatrix} \tag{9}$$

where n_{air} and n_{core} are the refractive index of air and core, respectively, and d is the cavity length. Matrix B can be obtained by concatenating the matrix of reflection and propagation. Then a series of processes that enter the cavity from the input fiber and transmit into the output fiber after n round-trips in the cavity, can be represented by the matrix.

Appendix C
Complex Beam Parameter

Complex beam parameter and its inverse are expressed as $q(z) = z + jz_0$ and $1/q(z) = 1/R(z) - j\lambda/\pi W(z)^2$, respectively. As shown in Section 2, q_0 in the input fiber can be obtained by calculating W_f. According to the standard formula for step-index fiber [23], W_f is affected by a and V-number V as shown in Eq. (10), where V is expressed as Eq. (11). Here, $n_{cladding}$ denote the refractive index of the cladding.

$$W_f = a(0.65 + 1.619V^{-1.5} + 2.87V^{-6}) \tag{10}$$

$$V = \frac{2\pi fa}{c}\sqrt{n_{core}^2 - n_{cladding}^2} \tag{11}$$

Assuming SMF-28, W_f can be expressed as a function of frequency by substituting a = 4.5 μm, $n_{core} = 1.4504$, $n_{cladding} = 1.4447$ into Eq. (10) and (11). Then, q_n can be finally obtained from q_0 and matrix $AB^{n-1}CD$ as shown in Eq. (12).

$$q_n = \frac{q_0 \times AB^{n-1}CD(1,1) + AB^{n-1}CD(1,2)}{q_0 \times AB^{n-1}CD(2,1) + AB^{n-1}CD(2,2)} \tag{12}$$

References

[1] J. Masson, R. St-Gelais, A. Poulin, and Y.-A. Peter, "Tunable fiber laser using a MEMS-based in plane Fabry-Pérot filter," *IEEE J. Quantum Electron.*, vol. 46, no. 9, pp. 1313–1319, Sep. 2010.
[2] H. Omran, Y. M. Sabry, M. Sadek, K. Hassan, M. Y. Shalaby, and D. Khalil, "Deeply-etched optical MEMS tunable filter for swept laser source applications," *IEEE Photon. Technol. Lett.*, vol. 26, no. 1, pp. 37–39, Jan. 2014.
[3] T. Wei, Y. Han, H.-L. Tsai, and H. Xiao, "Miniaturized fiber inline Fabry-Perot interferometer fabricated with a femtosecond laser," *Opt. Lett.*, vol. 33, no. 6, pp. 536–538, 2008.
[4] X. Zhou and Q. Yu, "Wide-range displacement sensor based on fiber-optic Fabry–Perot interferometer for subnanometer measurement," *IEEE Sens. J.*, vol. 11, no. 7, pp. 1602–1606, Jul. 2011.
[5] C.-L. Lee, W.-Y. Hong, H.-J. Hsieh, and Z.-Y. Weng, "Air gap fiber Fabry–Pérot interferometer for highly sensitive micro-airflow sensing," *IEEE Photon. Technol. Lett.*, vol. 23, no. 13, pp. 905–907, Jul. 2011.

[6] Y. Colombe, T. Steinmetz, G. Dubois, F. Linke, D. Hunger, and J. Reichel, "Strong atom–field coupling for Bose–Einstein condensates in an optical cavity on a chip," *Nature*, vol. 450, no. 7167, pp. 272–276, 2007.

[7] J. Gallego, W. Alt, T. Macha, M. Martinez-Dorantes, D. Pandey, and D. Meschede, "Strong Purcell effect on a neutral atom trapped in an open fiber cavity," *Phys. Rev. Lett.*, vol. 121, no. 17, 2018, Art. no. 173603.

[8] G. Pandey, E. T. Thostenson, and D. Heider, "Electric time domain reflectometry sensors for non-invasive structural health monitoring of glass fiber composites," *Prog. Electromagn. Res.*, vol. 137, pp. 551–564, 2013.

[9] Y. Kim and D. P. Neikirk, "Micromachined Fabry-Perot cavity pressure transducer," *IEEE Photon. Technol. Lett.*, vol. 7, no. 12, pp. 1471–1473, Dec. 1995.

[10] A. Wang, H. Xiao, J. Wang, Z. Wang, W. Zhao, and R. May, "Self-calibrated interferometric-intensity-based optical fiber sensors," *J. Lightw. Technol.*, vol. 19, no. 10, 2001, Art. no. 1495.

[11] C. Belleville and G. Duplain, "White-light interferometric multimode fiber-optic strain sensor," *Opt. Lett.*, vol. 18, no. 1, pp. 78–80, 1993.

[12] C. E. Lee and H. F. Taylor, "Fiber-optic Fabry-Perot temperature sensor using a low-coherence light source," *J. Lightw. Technol.*, vol. 9, no. 1, pp. 129–134, 1991.

[13] Y. Zhu, Z. Huang, F. Shen, and A. Wang, "Sapphire-fiber-based white-light interferometric sensor for high-temperature measurements," *Opt. Lett.*, vol. 30, no. 7, pp. 711–713, 2005.

[14] O. Kilic, M. J. Digonnet, G. S. Kino, and O. Solgaard, "Asymmetrical spectral response in fiber Fabry–Perot interferometers," *J. Lightw. Technol.*, vol. 27, no. 24, pp. 5648–5656, 2009.

[15] P. R. Wilkinson and J. R. Pratt, "Analytical model for low finesse, external cavity, fiber Fabry–Perot interferometers including multiple reflections and angular misalignment," *Appl. Opt.*, vol. 50, no. 23, pp. 4671–4680, 2011.

[16] Y. M. Sabry, D. Khalil, B. Saadany, and T. Bourouina, "In-plane external fiber Fabry–Perot cavity comprising silicon micromachined concave mirror," *J. Micro-Nanolithogr. MEMS MOEMS*, vol. 13, no. 1, 2013, Art. no. 011110.

[17] D. Kleckner, W. T. M. Irvine, S. S. R. Oemrawsingh, and D. Bouwmeester, "Diffraction-limited high-finesse optical cavities," *Phys. Rev. A*, vol. 81, no. 4, pp. 1–5, 2010, Art. no. 043814.

[18] J. Benedikter *et al.*, "Transverse-mode coupling and diffraction loss in tunable Fabry–Pérot microcavities," *New J. Phys.*, vol. 17, no. 5, pp. 1–9, 2015, Art. no. 053051.

[19] A. G. Fox and T. Li, "Resonant modes in a maser interferometer," *Bell Syst. Techn. J.*, vol. 40, no. 2, pp. 453–488, 1961.

[20] T. Li, "Diffraction loss and selection of modes in maser resonators with circular mirrors," *Bell Syst. Techn. J.*, vol. 44, no. 5, pp. 917–932, 1965.

[21] G. Son and K. Yu, "Radiation from concave optical fiber tips fabricated by laser induced photothermal effects," in *Proc. IEEE Int. Symp. Antennas Propag.*, 2018, pp. 1–2.

[22] J. Choi, G. Son, Y. Jin, and K. Yu, "Ultra-small optical fiber fabry-pérot cavities fabricated by laser-induced photothermal effect," in *Proc. IEEE Opt. Fiber Commun. Conf. Exhib.*, 2020, pp. 1–3.

[23] D. Marcuse, "Loss analysis of single-mode fiber splices," *Bell Syst. Techn. J.*, vol. 56, no. 5, pp. 703–718, 1977.